Journal of Magnetism and Magnetic Materials 589 (2024) 171548

Contents lists available at ScienceDirect

Journal of Magnetism and Magnetic Materials

journal homepage: www.elsevier.com/locate/jmmm

Research article

Magnetoresitance vs. electronic structure in Cu doped single crystalline Bi_2Se_3 3D topological insulator

Maciej Chrobak [a,b,*], Krzysztof Maćkosz [c,a,b], Kamil Nowak [a,b], Andrii Naumov [b], Marek Przybylski [a,b]

[a] Faculty of Physics and Applied Computer Science, AGH University of Krakow, Mickiewicza Av. 30, 30-059, Krakow, Poland
[b] Academic Centre for Materials and Nanotechnology, AGH University of Krakow, Mickiewicza Av. 30, 30-059, Krakow, Poland
[c] Empa-Swiss Federal Laboratories for Materials Science and Technology, Laboratory for Mechanics of Materials and Nanostructures, Feuerwerkerstrasse 39, CH-3602, Thun, Switzerland

ARTICLE INFO

Keywords:
Topological insulators
Surface states
Schubnikov de-Haas oscillations
STM
STS
ARPES

ABSTRACT

Bismuth selenide (Bi_2Se_3) is one of the 3D topological insulators (TI) that can be characterised as materials of a semiconducting volume and a conductive surface. The evolution of the electronic structure of $(Bi_{1-x}Cu_x)_2Se_3$ (x = 0, 0.025, 0.05, 0.09 and 0.125) was investigated by angle-resolved photoemission spectroscopy (ARPES), scanning tunnelling microscopy (STM/STS) and Shubnikov-de Haas oscillations (SdH). The results show that doping with Cu does not change the electronic structure, in particular it does not destroy the nontrivial topology of the system. The lack of superconductivity is discussed in view of intercalated $Cu_xBi_2Se_3$ in which superconductivity is observed.

1. Introduction

Topological insulators (TI) are a relatively new type of materials and one of the most exciting and studied systems in condensed matter physics today. This great interest is due to the new exotic properties resulting from the non-trivial topology bulk states, the presence of which results in gapless topological surface states (TSS) [1–3]. Such topological surface states are located inside the bulk band gap. TSS has a helical spin texture and obey the linear energy dispersion relation i.e. they must be filled by massless Dirac fermions [4]. As a consequence of this fact, the electrons in TSS have the π Berry phase after moving through a closed trajectory around the Fermi surface [5]. The Dirac cone-like TSS in the bulk energy gap was recognised by angle resolved photoemission spectroscopy (ARPES) and scanning tunnelling microscopy (STM) [6,7]. This complicated electronic structure of TIs leads to the occurrence of many interesting properties which can be observed in electronic transport, such as nonsaturating linear magnetoresistance, Shubnikov-de Haas (SdH) oscillations, high carrier mobility [8] and the superconducting proximity effect [9]. Combining a TI with s-wave superconductors will make it possible to realise the topological superconductivity associated with Majorana fermions [3,4,10]. Majorana particle is a fermion that is its own antiparticle. If Majorana particles are spatially localised, they emerge as Majorana zero modes and follow non-Abelian statics, which is necessary for topological quantum computation [11].

Majorana fermions and Majorana zero modes occur also in topological superconductors (TSC) [10]. However, the realisation of a topological superconductor is very rare. One of the candidates to be a TSC is $Cu_xBi_2Se_3$ [12], but as yet there is still no consensus that it is a topological superconductor. Low-temperature STM studies have observed a full superconducting gap without in-gap states or a zero bias conductance peak which should be present if the material hosts Majorana fermions [13]. On the other hand, a spin-rotation symmetry breaking in a superconducting state has been discovered by an NMR study of $Cu_xBi_2Se_3$ [14]. This means that the Cooper pairs are in a pseudo-spin–triplet state with a pinned *d*-vector direction, which suggests $Cu_xBi_2Se_3$ as an odd-parity TSC state [15].

Although much research has been done on this topic, it is still not entirely clear what is responsible for the occurrence of this unconventional superconductivity. In this paper we want to shed some light on the evolution of the Fermi surface of $(Bi_{1-x}Cu_x)_2Se_3$ (x = 0, 0.025, 0.05, 0.09 and 0.125) by means of angle resolved photoemission spectroscopy (ARPES), scanning tunnelling spectroscopy (STS) and Shubnikov-de Haas oscillations (SdH) studies. Moreover, we want to check whether the results obtained by 3 different techniques are consistent with each other. The last aim of this paper is to check if superconductivity occurs in samples where Cu substitutes Bi instead of intercalation in the van der Waals gap.

* Corresponding author at: Faculty of Physics and Applied Computer Science, AGH University of Krakow, Mickiewicza Av. 30, 30-059, Krakow, Poland.
E-mail address: mchrobak@agh.edu.pl (M. Chrobak).

https://doi.org/10.1016/j.jmmm.2023.171548
Received 7 August 2023; Received in revised form 31 October 2023; Accepted 19 November 2023
Available online 20 November 2023

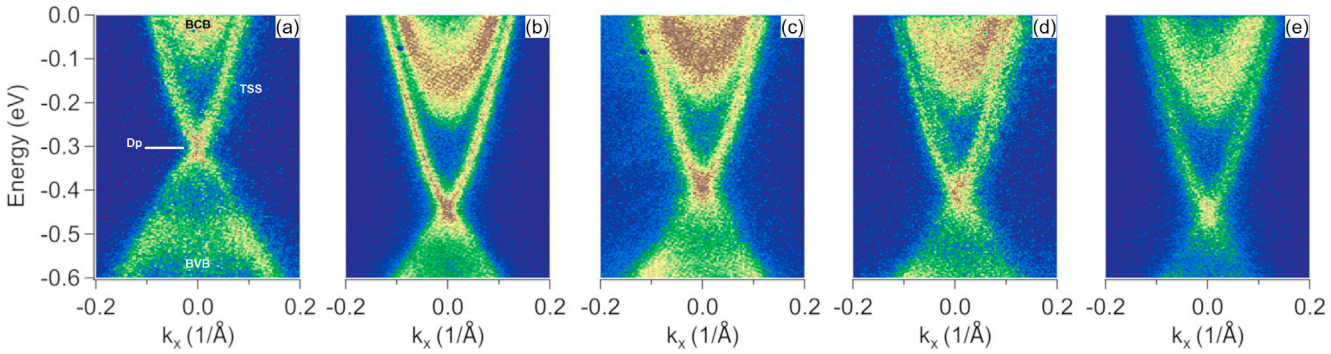

Fig. 1. ARPES intensity spectra measured in the K–Γ–K direction of the reciprocal space (a) Bi_2Se_3, (b) $(Bi_{0.975}Cu_{0.025})_2Se_3$, (c) $(Bi_{0.95}Cu_{0.05})_2Se_3$, (d) $(Bi_{0.91}Cu_{0.09})_2Se_3$ and (e) $(Bi_{0.875}Cu_{0.125})_2Se_3$.

2. Material and methods

The subject of the research are single crystals of Cu-doped bismuth selenium $(Bi_{1-x}Cu_x)_2Se_3$ where x varies from 0 to 0.125. The samples were synthesised using the Bridgman method. In the synthesis process, elements of 5N purity were deoxidised in carbon boats in a two-zone horizontal furnace in vacuum of 10^{-7} mbar and then further purified by multiple vacuum distillations under a dynamic vacuum of 10^{-7} mbar until they reached 7N purity [16]. The nominal compositions of $(Bi_{1-x}Cu_x)_2Se_3$ (x = 0, 0.025, 0.05, 0.09 and 0.125) were weighted and then the initial synthesis was carried out on the same boats at 1170 K, after which the material was slowly cooled under controlled Se vapour pressure. Then, the initially synthesised material was transferred to a quartz ampule that, after air evacuation, was placed in a three-zone vertical furnace. The temperature gradient in the growth zone was set at 0.5 K/cm. The ampule velocity across the growth zone was 0.5 to 1.5 mm/h. As a result, the samples were contamination-free and easily cleavable along the a-b plane.

The ARPES measurements were performed at the UARPES beamline of NSRC Solaris under a pressure lower than 1×10^{-10} mbar using horizontally polarised undulator radiation. Photoelectrons were detected with a VG-Scienta DA30L electron energy analyser. The overall resolutions of the ARPES measurements were 8 meV (energy) and 0.1 deg (angular). The samples were glued with epoxy resin to a sample holder and cleaved in situ in a load-lock chamber at a pressure better than 1×10^{-7} mbar. The measurements were carried out immediately after cleaving and cooling to 12 K having in mind the ageing effect of the sample surface.

The topography and electronic structure at the surface were probed using a variable temperature scanning tunnelling microscope (VT STM) with an RHK Beetle scan head. Prior to the STM/STS measurements the samples were cleaved in-situ in ultra high vacuum ($<1 \times 10^{-8}$ mbar), at room temperature, resulting in an atomically clean surface. The electronic structure at the surface was probed by STS. An electrochemically etched tungsten tip was used. The STS technique allows to measure the tunnelling current (I_T) and differential tunnelling conductivity ($\frac{dI_T}{dV}$) as a function of the bias voltage, which is a measure of the local density of states (LDOS). Since I_T, and thus also $\frac{dI_T}{dV}$, depends on the actual tunnelling conditions between the surface to be tested and the STM tip [17], the gathered spectra $\frac{dI_T}{dV}$ were normalised to the total conductance $\frac{I}{V}$ [17]. The STM and STS measurements were carried out under UHV conditions at a temperature of around 36 K. The differential tunnelling conductance ($\frac{dI_T}{dV}$) was obtained using a standard lock-in technique with a modulation amplitude of 20 mV and a frequency of 12.3 kHz.

The electronic transport measurements were performed on samples of the shape of a classic Hall bar. The electronic contacts between the samples and the experimental setup were made with a silver paste. The transport measurements were carried out in a TRITON dilution refrigerator using a Nanonis Tramea quantum transport measurement system with a lock-in amplifier. The modulation frequency for all the tests was set at 17.8 Hz. The resistivity versus temperature was measured for temperatures from 100 mK to 25 K. The dependence of the longitudinal and transverse resistivity on the magnetic field was probed up to 14 T at various temperatures from 100 mK to 5 K.

3. Results and discussion

Experimental techniques such as ARPES and STM (especially in the spectroscopy mode) are frequently used to test whether material exhibits a non-trivial topology. This is because these techniques are surface sensitive and can directly probe topological surface states. We measured ARPES intensity spectra to verify single-crystallinity and the presence of the topological surface states in our samples. In Figs. 1(a–e) we show the ARPES intensity spectra measured at 12 K in K–Γ–K direction of the reciprocal space, which provide information on the electronic structure at the surface and a few atomic layers beneath it. For all the samples we measured, well-defined spectra of the band structure were detected, which prove that the samples are single crystalline. All the spectra reveal valence and conduction volume bands (BVB and BCB, respectively) and Dirac cone-like topological surface states (TSS), which prove that replacing the Bi atoms with Cu does not destroy the non-trivial topology of the samples, at least up to x = 0.125. Furthermore, doping does not change the electronic structure with respect to pristine Bi_2Se_3 except for shifting the position of the Fermi level deeper into the BCB, i.e., it increases the carrier concentration. Additionally, the Dirac point (DP), which is located near the top of the BVB (as marked in Fig. 1(a)), is visible for each sample. The measurements show that the density of states is the lowest at the DP, as expected.

From the measured STS spectra, the Fermi wave vector (k_F) was obtained as half of the diameter of the circular area between the edges of the TSS cone at the Fermi level. Next the Fermi velocity (v_F) in the vicinity of the Fermi energy (E_F) was calculated from the linear part of the dispersion relation using the formula (1):

$$E(k) = \hbar \cdot v_F \cdot k \Rightarrow v_F = \frac{1}{\hbar}\left(\frac{dE}{dk}\right). \quad (1)$$

Knowing k_F and v_F the effective mass (m_{eff}) was calculated from the formula (2):

$$m_{eff} = \frac{\hbar k_F}{v_F}. \quad (2)$$

The parameters of the electronic structure obtained from the ARPES measurements are listed in Table 1.

To examine the surface quality of the single-crystalline samples on atomic scale, STM measurements were performed. The topography of all the prepared samples was investigated at 36 K using STM. Atomically clean surfaces with a hexagonal symmetry were observed confirming the high-quality of the single-crystalline samples. We did

Table 1
The values of the Fermi wave vectors (k_F), the Fermi velocities (v_F), effective masses (m_{eff}) and energy difference between the Fermi level (E_F) and the Dirac point (E_{DP})for the $(Bi_{1-x}Cu_x)_2Se_3$ where (x = 0, 0.025, 0.05, 0.09, 0.125) obtained from the ARPES experiment at 12 K.

x	k_F [Å^{-1}]	v_F [10^5 $\frac{m}{s}$]	m_{eff} [m_e]	E_F-E(D_p) [meV]
0	0.093	5.72	0.094	300
0.025	0.130	5.87	0.127	441
0.05	0.120	5.84	0.119	395
0.09	0.123	5.91	0.120	409
0.125	0.133	6.03	0.126	455

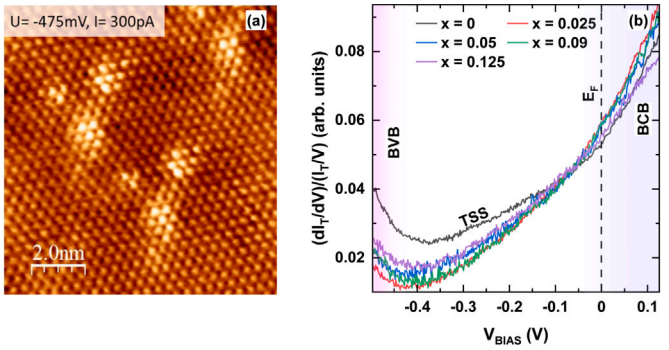

Fig. 2. (a) 10 x 10 nm STM topography scan of Bi_2Se_3 obtained at $V_{BIAS} = -475$ mV and I = 300 pA measured at 36 K. (b) Normalised STS spectra of $(Bi_{1-x}Cu_x)_2Se_3$ measured at 36 K. The regions of the BVB, BCB, and TSS are marked with the magenta, blue, and white background, respectively. The colour gradient reflects the uncertainty in determining the boundary of the bands.

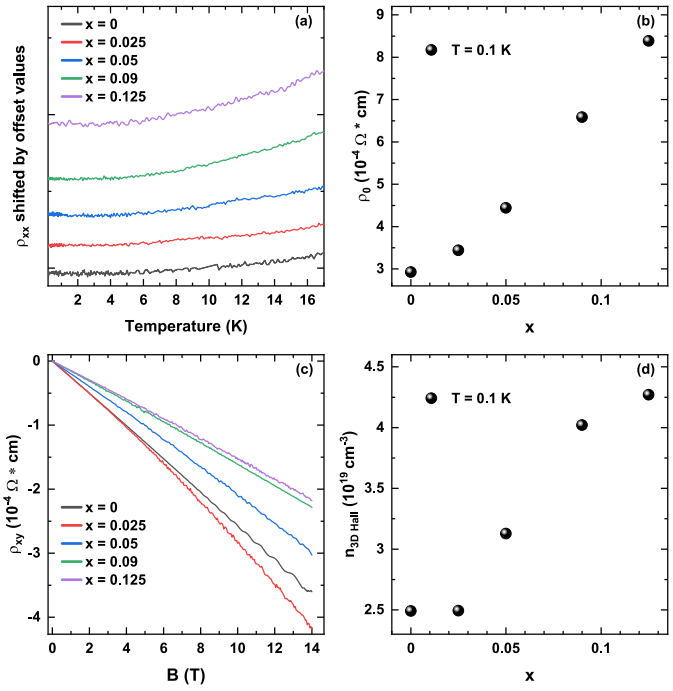

Fig. 3. (a) Dependence of resistivity vs. temperature. (b) The value of the residual resistivity (ρ_0) as a function of the Cu content measured at 100 mK. (c) Dependence of transverse resistivity versus magnetic field at 100 mK. (d) Carrier concentration obtained after fitting the single-band model of the $(Bi_{1-x}Cu_x)_2Se_3$ where (x = 0, 0.05, 0.1, 0.18, 0.25).

not observe any significant differences between the samples and therefore, in Fig. 2(a), we show only the STM image obtained for the undoped sample. This representative topography scan shows a characteristic point defect with a triangular shape, which corresponds to the substitution of Bi with Se in the fifth atomic layer [18,19]. Defects of this type reduce carrier concentration [19,20].

In Fig. 2(b) we show the normalised STS spectra ($\frac{dI_T/dV}{I/V}$) for all samples. Normalisation was perfomed because the tunnelling current depends both on the electronic structure of the surface being tested and on the electronic structure of the tip [17]. The $\frac{dI_T}{dV}$ spectra were normalised by dividing the differential conductance $\frac{dI_T}{dV}$ by the total conductance $\frac{I_T}{V}$, i.e. $\frac{dI_T/dV}{I/V}$ [17]. The divergence problem at small bias voltages in the case of $\frac{dI_T/dV}{I/V}$ was overcome by broadening ΔV up to 1.2 V [21]. For each sample, the upper edge of the BVB and the lower edge of the BCB are clearly visible. The finite density of states inside the bulk energy gap is due to the TSS that are characterised by a linear energy dispersion. The spectrum of the pristine Bi_2Se_3 is of n-type, as expected [22]. In Bi_2Se_3, unlike e.g. in Bi_2Te_3, the Dirac cone is entirely located in the bulk band gap, so the Dirac point should correspond to the lowest density of states (like in the ARPES spectra). And this is the case: since the normalised STS signal is proportional to LDOS, the minimum of the STS spectra corresponds to the lowest density of states, which implies that the minimum of the STS is the Dirac point. Therefore, if we determine the position of the STS minimum, we determine the energy difference between the Dirac point and the Fermi level (E_F corresponds to $V_{BIAS} = 0$). For the pristine sample, the energy difference between the DP and E_F is 349 meV. By adding a Cu dopant on the level of x = 0.025, the difference $|E_F - E_{DP}|$ increases up to 419 meV. However, further increasing the Cu content does not cause a further shift of the DP with respect to E_F.

The resistance versus temperature below 30 K and the Hall voltage versus magnetic field at 100 mK were measured to characterise preliminary electronic transport properties of the synthesised samples. The results of the R(T) measurements are shown in Fig. 3(a). Each measured sample exhibits a metallic character, i.e. the resistance decreases with decreasing temperature. Below 5 K, the R(T) shows a saturation implying a finite residual resistivity (ρ_0). No superconducting transition in the resistance is observed down to 100 mK for all the measured samples. In Fig. 3(b) we show the residual resistivity as a function of Cu doping. The residual resistivity increases with the content of Cu, which is interpreted as a result of enhanced (more frequent) electron scattering due to an increasing number of defects in the crystallographic structure caused by doping.

In Fig. 3(c) we present the results of the Hall effect measurements. All measured samples have a negative linear dependence of transverse resistivity on the external magnetic field, i.e. the dominant carriers are electrons. The slope of the measured transverse resistivity decreases with increasing the content of Cu (except for $x = 0.025$). It means that the Hall constant (R_H), which is proportional to the slope of transverse resitivity, decreases and thus the carrier concentration ($n = 1/R_H e$) increases with increasing the doping with Cu. In Fig. 3(d), we present carrier concentrations obtained after linear fitting of the measured transverse resistivity at 100 mK in the magnetic field below 4 T, so quantum oscillations do not affect the values being fitted. The carrier concentration increases from 2.5×10^{19} cm^{-3} for the undoped sample to 4.55×10^{19} cm^{-3} for the sample with the highest content of Cu, which proves that Cu adds electrons to the system.

The field dependence of resistivity was measured in the external magnetic field up to 14 T at several temperatures from 100 mK to 5 K. The magnetic field was set perpendicular to the a–b plane of the samples. In Fig. 4 we show the magnetoresistance (MR) for all the samples measured at 100 mK. The MR was calculated using the formula (3):

$$MR = \frac{R(B) - R(0)}{R(0)} \cdot 100\%, \quad (3)$$

where R is resistance and B is external magnetic field. For all the samples we observe Shubnikov-de Haas quantum oscillations (SdH). Analysis of SdH allows to derive some parameters of the electronic

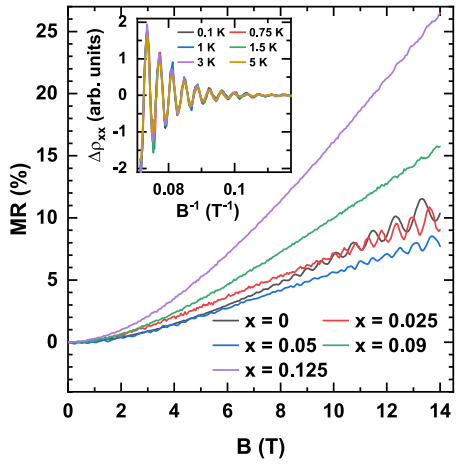

Fig. 4. Magnetoresistance of $(Bi_{1-x}Cu_x)_2Se_3$ (x = 0, 0.025, 0.05, 0.09, 0.125) measured at 100 mK. The inset shows the SdH oscillations as a function of the inverse magnetic field of $(Bi_{0.975}Cu_{0.025})_2Se_3$ measured at several temperatures.

structure, such as k_F, m_{eff} and E_F. Unlike STM/STS and ARPES which offer information mostly from the surface, quantum oscillations provide information obtained at the extremal Fermi surface, which comprises bulk and surface states. Pure SdH oscillations ($\Delta\rho_{xx}$) were extracted from the field dependence of resistivity by subtracting the polynomial background. In the inset to Fig. 4, we show the resulting SdH oscillations for the sample $(Bi_{0.975}Cu_{0.025})_2Se_3$ measured at several temperatures. Also for the remaining samples, the SdH oscillations of singular frequency are obtained. The amplitude of the oscillations decreases with increasing temperature, which proves that the observed oscillations are Shubnikov-de Haas quantum oscillations.

The frequency of the SdH oscillations was obtained from their Fast Fourier Transforms (FFT). In Fig. 5(a) we show the normalised FFT amplitude for all the samples. The FFT amplitude was normalised to its maximum value. For each sample, we can distinguish one dominating peak corresponding to the frequency of the SdH oscillations. The frequency of the SdH oscillations is directly related to the cross section $A(E_F)$ of the extremal Fermi surface according to the Onsager relation:

$$f_{SdH} = \left(\frac{\hbar}{2\pi e}\right) A(E_F). \tag{4}$$

Then, if we assume a spherical Fermi surface, we can calculate the Fermi wave vector: $k_F = \sqrt{\frac{A(E_F)}{\pi}}$. The obtained values of k_F are plotted in Fig. 5(b) as black points. For the pristine sample, the Fermi wave vector is 0.07 $Å^{-1}$ and is comparable to the values reported in the literature [3,23]. As a result of doping with Cu, we observe that k_F increases by approximately 30 % for the x = 0.025 sample. The effect is similar to that observed for doping with Fe [24–26]. Further doping with Cu does not cause further changes of the Fermi wave vector. This may suggest that additional Cu atoms start to precipitate in the van der Waals space between the quintuple layers. The values of k_F obtained from the quantum oscillations are compared to the values obtained from the ARPES measurements (the red points in Fig. 5(b)) which show the same tendency. It is, however, true that there are discrepancies in the absolute values of k_F obtained from both methods. Such a lack of quantitative agreement is not surprising having in mind that the SdH oscillations were detected at 100 mK, whereas the ARPES experiment was carried out at 12 K. Moreover, the ARPES experiment is sensitive to the band bending of the electronic bands near the surface which influences the values of the Fermi wave vector.

Another parameter that can be determined from the SdH oscillations is the effective mass. For this purpose, the Lifshitz-Kosevich theory (LK) [27] was applied. Accordingly, the effective mass can be determined from the temperature damping factor R_T which is given by the formula:

$$R_T = \frac{2\pi^2\left(\frac{k_B T}{\hbar\omega_c}\right)}{\sinh\left[2\pi^2\left(\frac{k_B T}{\hbar\omega_c}\right)\right]}, \tag{5}$$

where ω_c is the cyclotron frequency. Therefore, the temperature dependence of $\Delta\rho_{xx}$ can be expressed as:

$$\Delta\rho_{xx}(T) = \Delta\rho_{xx}(0)\frac{\lambda(T)}{\sinh(\lambda(T))}, \tag{6}$$

where $\lambda(T) = 14.69\ \frac{m_{eff}T}{m_e B}$ [3]. So we can find m_{eff} by fitting the function (6) to the measured $\Delta\rho_{xx}(T)$. In Fig. 5(c) we show the values of m_{eff} (the black points) obtained from the fitting and the effective mass values obtained from the ARPES experiment. The results obtained from both methods agree with each other, i.e., m_{eff} increases with increasing the Cu doping. Since doping increases carrier concentration, this is also consistent with calculations of the effective mass as a function of carrier concentration available in the literature [20,28]. Slight differences in the m_{eff} values obtained from SdH and ARPES methods result from the same reasons as in the case of k_F, i.e., from different temperatures at which the SdH and ARPES experiments were carried out.

Finally, knowing the Fermi wave vector and the effective mass from the SdH oscillations we were able to calculate the Fermi velocity and the Fermi energy which are related to each other by Eq. (7):

$$m_{eff} = E_F v_F^2 = \frac{\hbar k_F}{v_F}. \tag{7}$$

In Fig. 5(d), we show the Fermi level energy calculated from the SdH oscillations (the black points), determined from the ARPES measurements (the red points) and derived from the STS spectra (the blue points). From the results obtained from the SdH oscillations and ARPES measurements, it seems that the Fermi energy and k_F vs. Cu doping behave similarly, i.e., a small content of Cu changes E_F by approximately 40%. Further increasing of the Cu content does not cause any further changes. From the STS spectra, the change of E_F with increasing the content of Cu is also observed (20%), but it is smaller compared to the results of the SdH and ARPES experiments (40%). This difference relates to the different temperatures at which our experiments were performed and to the fact that STS was not averaged over a large sample area but probed locally at the undefected surface.

In general, all three experimental techniques (ARPES, STS and SdH) applied for the materials reported in this manuscript confirm that the non-trivial topological surface states are preserved for all the measured samples. The Dirac cone originating from the surface states of the linear dispersion relation is clearly visible from the ARPES study and from the STS experiment. The SdH oscillations originating from the non-trivial topology are visible for all the samples. These mean that doping does not change electronic structure. However, doping increases the carrier concentration. This result is similar to what is shown for the Cu-intercalated samples $Cu_xBi_2Se_3$ in the literature [29]. The similarity between the results for all our samples, i.e., the samples with Cu substituting Bi and the $Cu_xBi_2Se_3$ samples, where Cu occupies a position in the gap between the quintuples, may indicate that in the case of our $(Bi_{1-x}Cu_x)_2Se_3$ samples, a portion of Cu atoms may be located in the van der Waals gap.

Finally, we checked whether our samples are superconducting or not. Unfortunately, we did not detect transition to the superconducting state by measuring the resistance versus temperature down to 70 mK. The main reason for this discrepancy may be that in our $(Bi_{1-x}Cu_x)_2Se_3$ samples Cu substitutes Bi, but in the $Cu_xBi_2Se_3$ superconductive samples [12,29] Cu is intercalated into the van der Waals gap. Also, for our samples the carrier concentration is found on the level of 10^{19} whereas for the superconductive samples the carrier concentration is

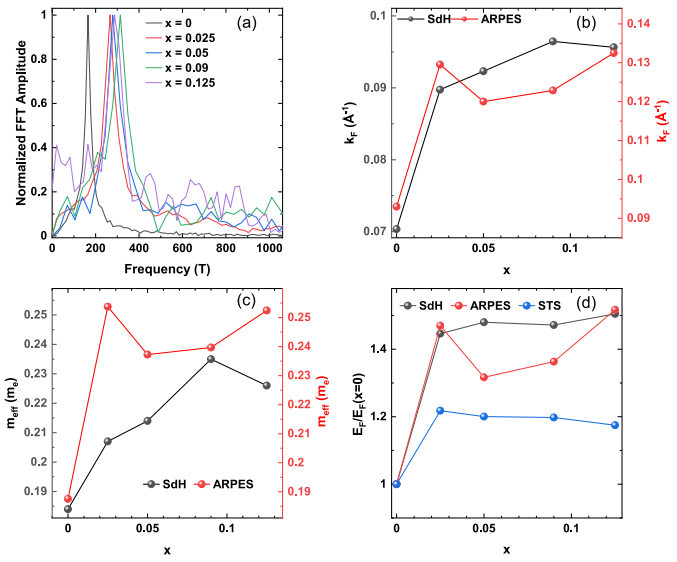

Fig. 5. (a) Normalised fast Fourier transform amplitude of the SdH oscillations of $(Bi_{1-x}Cu_x)_2Se_3$ (x = 0, 0.025, 0.05, 0.09, 0.125) measured at 100 mK. (b) Fermi wave vector as a function of Cu doping. (c) Effective mass as a function of Cu doping. (d) Fermi level energy calculated with respect to the energy of the Dirac point normalised to the Fermi level energy for undoped sample. (b – d) The black points are obtained from the quantum oscillations, the red points are obtained from ARPES, and the blue points are obtained from the STS data.

reported on the level of 10^{20}, which may be the reason for the lack of superconductivity in our samples. Such a low concentration of carriers in our samples is caused by the large number of structural defects reducing the number of electrons in the system. Neither the ARPES nor the STM/STS measurements were able to provide information on the opening of the superconducting gap because they were applied at temperatures of 12 K and 36 K, respectively, which are clearly above the critical temperature reported for the intercalated superconducting samples [12,29].

4. Conclusions

All the experimental techniques applied to obtain the results discussed in this article, i.e. the ARPES, STM/STS and magnetoresistance measurements (allowing the detection of SdH quantum oscillations), prove that the doping of Bi_2Se_3 with Cu does not destroy the non-trivial topology of the electronic states and the non-trivial topological surface states remain preserved. Both, in the ARPES and STS spectra for all the measured samples the topological surface states in the form of a Dirac cone (linear dispersion) were clearly visible. The SdH oscillations of well-defined frequency were detected. The doping of Bi_2Se_3 with Cu does not significantly alter the electronic structure. However, k_F, m_{eff} and the distance between the E_F and E_{DP} are found to be significantly increased with respect to the undoped sample as a result of increasing the carrier concentration. This observation (as well as the parameters of the electronic structure) is similar to the literature data on $Cu_xBi_2Se_3$ intercalated samples. This could mean that a portion of Cu atoms is located in the van der Waals gap also in the case of our $(Bi_{1-x}Cu_x)_2Se_3$ samples, although it is insufficient to induce superconductivity: no superconductivity was observed down to 70 mK. It seems that the presence of Cu atoms in the van der Waals gap is necessary to establish superconductivity, most likely due to the hybridisation of the Cu-d orbitals with the s-orbitals of Se. Cu-Se bonding seems to play a crucial role for superconductivity. The dominant Cu-Se bonding is expected to be accompanied by the removal of the van der Waals gap (resulting in volume conductivity) which is definitely not the case for our $(Bi_{1-x}Cu_x)_2Se_3$ samples.

CRediT authorship contribution statement

Maciej Chrobak: Conceptualization, Methodology, Validation, Investigation, Visualization, Writing – original draft. **Krzysztof Maćkosz:** Investigation. **Kamil Nowak:** Investigation. **Andrii Naumov:** Investigation, Visualization. **Marek Przybylski:** Supervision, Validation, Writing – review & editing.

Declaration of competing interest

The authors declare that they have no known competing financial interests or personal relationships that could have appeared to influence the work reported in this paper.

Data availability

Data will be made available on request.

Acknowledgements

This work was financially supported by the National Science Centre, Poland Grant 2018/02/X/ST3/03220 and by the programme "Excellence initiative - research university" for the AGH University of Science and Technology.

K. N. was partly supported by the EU Project POWR.03.02.00-00-I004/16.

This publication was developed under the provision of the Polish Ministry of Education and Science project "Support for research and development with the use of research infrastructure of the National Synchrotron Radiation Centre SOLARIS" under contract nr 1/SOL/2021/2. We acknowledge the SOLARIS Centre for access to the Beamline URANOS, where the measurements were performed, and thank N. Olszowska and M. Rosmus for their assistance.

Appendix A. Supplementary data

Supplementary material related to this article can be found online at https://doi.org/10.1016/j.jmmm.2023.171548.

References

[1] P. Roushan, J. Seo, C.V. Parker, Y.S. Hor, D. Hsieh, D. Qian, A. Richardella, M.Z. Hasan, R.J. Cava, A. Yazdani, Topological surface states protected from backscattering by chiral spin texture, Nature 460 (7259) (2009) 1106–1109, http://dx.doi.org/10.1038/nature08308.

[2] J.E. Moore, The birth of topological insulators, Nature 464 (7286) (2010) 194–198, http://dx.doi.org/10.1038/nature08916.

[3] Y. Ando, Topological insulator materials, J. Phys. Soc. Japan 82 (10) (2013) 102001, http://dx.doi.org/10.7566/JPSJ.82.102001.

[4] M.Z. Hasan, C.L. Kane, Colloquium: Topological insulators, Rev. Modern Phys. 82 (4) (2010) 3045–3067, http://dx.doi.org/10.1103/RevModPhys.82.3045.

[5] J.G. Analytis, R.D. McDonald, S.C. Riggs, J.-H. Chu, G.S. Boebinger, I.R. Fisher, Two-dimensional surface state in the quantum limit of a topological insulator, Nat. Phys. 6 (12) (2010) 960–964, http://dx.doi.org/10.1038/nphys1861.

[6] Y.L. Chen, J.G. Analytis, J.-H. Chu, Z.K. Liu, S.-K. Mo, X.L. Qi, H.J. Zhang, D.H. Lu, X. Dai, Z. Fang, S.C. Zhang, I.R. Fisher, Z. Hussain, Z.-X. Shen, Experimental realization of a three-dimensional topological insulator, Bi_2Te_3, Science 325 (5937) (2009) 178–181, http://dx.doi.org/10.1126/science.1173034.

[7] Z. Alpichshev, J.G. Analytis, J.-H. Chu, I.R. Fisher, Y.L. Chen, Z.X. Shen, A. Fang, A. Kapitulnik, STM imaging of electronic waves on the surface of Bi_2Te_3: Topologically protected surface states and hexagonal warping effects, Phys. Rev. Lett. 104 (2010) 016401, http://dx.doi.org/10.1103/PhysRevLett.104.016401.

[8] S. Sharma, S. Kumar, G.C. Tewari, G. Sharma, E.F. Schwier, K. Shimada, A. Taraphder, C.S. Yadav, Magnetotransport and high-resolution angle-resolved photoelectron spectroscopy studies of palladium-doped Bi_2Te_3, Phys. Rev. B 105 (11) (2022) 115120, http://dx.doi.org/10.1103/PhysRevB.105.115120.

[9] S. Ghatak, O. Breunig, F. Yang, Z. Wang, A.A. Taskin, Y. Ando, Anomalous fraunhofer patterns in gated josephson junctions based on the bulk-insulating topological insulator $BiSbTeSe_2$, Nano Lett. 18 (8) (2018) 5124–5131, http://dx.doi.org/10.1021/acs.nanolett.8b02029.

[10] X.-L. Qi, S.-C. Zhang, Topological insulators and superconductors, Rev. Modern Phys. 83 (4) (2011) 1057–1110, http://dx.doi.org/10.1103/RevModPhys.83.1057.

[11] S.D. Sarma, M. Freedman, C. Nayak, Majorana zero modes and topological quantum computation, npj Quantum Inf. 1 (1) (2015) http://dx.doi.org/10.1038/npjqi.2015.1.

[12] Y.S. Hor, A.J. Williams, J.G. Checkelsky, P. Roushan, J. Seo, Q. Xu, H.W. Zandbergen, A. Yazdani, N.P. Ong, R.J. Cava, Superconductivity in $Cu_xBi_2Se_3$ and its implications for pairing in the undoped topological insulator, Phys. Rev. Lett. 104 (2010) 057001, http://dx.doi.org/10.1103/PhysRevLett.104.057001.

[13] N. Levy, T. Zhang, J. Ha, F. Sharifi, A.A. Talin, Y. Kuk, J.A. Stroscio, Experimental evidence for *s*-wave pairing symmetry in superconducting $Cu_xBi_2Se_3$ single crystals using a scanning tunneling microscope, Phys. Rev. Lett. 110 (2013) 117001, http://dx.doi.org/10.1103/PhysRevLett.110.117001.

[14] K. Matano, M. Kriener, K. Segawa, Y. Ando, G.-q. Zheng, Spin-rotation symmetry breaking in the superconducting state of $Cu_xBi_2Se_3$, Nat. Phys. 12 (9) (2016) 852–854, http://dx.doi.org/10.1038/nphys3781.

[15] J.W.F. Venderbos, V. Kozii, L. Fu, Odd-parity superconductors with two-component order parameters: Nematic and chiral, full gap, and Majorana node, Phys. Rev. B 94 (2016) 180504, http://dx.doi.org/10.1103/PhysRevB.94.180504.

[16] H. Cao, S. Xu, I. Miotkowski, J. Tian, D. Pandey, M.Z. Hasan, Y.P. Chen, Structural and electronic properties of highly doped topological insulator Bi_2Se_3 crystals, Phys. Status Solidi-R 7 (2013) 133–135.

[17] J. Bardeen, Tunnelling from a many-particle point of view, Phys. Rev. Lett. 6 (1961) 57–59, http://dx.doi.org/10.1103/PhysRevLett.6.57.

[18] J. Dai, D. West, X. Wang, Y. Wang, D. Kwok, S.-W. Cheong, S.B. Zhang, W. Wu, Toward the intrinsic limit of the topological insulator Bi_2Se_3, Phys. Rev. Lett. 117 (2016) 106401, http://dx.doi.org/10.1103/PhysRevLett.117.106401.

[19] M. Jurczyszyn, M. Sikora, M. Chrobak, L. Jurczyszyn, Studies of surface states in Bi2Se3 induced by the BiSe substitution in the crystal subsurface structure, Appl. Surf. Sci. 528 (2020) 146978, http://dx.doi.org/10.1016/j.apsusc.2020.146978.

[20] B. Wiendlocha, Resonant levels, vacancies, and doping in Bi_2Te_3, Bi_2Te_2Se, and Bi_2Se_3 tetradymites, J. Elec. Materi. 45 (7) (2016) 3515–3531, http://dx.doi.org/10.1007/s11664-016-4502-9.

[21] R.M. Feenstra, Tunneling spectroscopy of the (110) surface of direct-gap III-V semiconductors, Phys. Rev. B 50 (1994) 4561–4570, http://dx.doi.org/10.1103/PhysRevB.50.4561.

[22] H. Zhang, C.-X. Liu, X.-L. Qi, X. Dai, Z. Fang, S.-C. Zhang, Topological insulators in Bi_2Se_3, Bi_2Te_3 and Sb_2Te_3 with a single Dirac cone on the surface, Nat. Phys. 5 (6) (2009) 438–442, http://dx.doi.org/10.1038/nphys1270.

[23] M. Petrushevsky, E. Lahoud, A. Ron, E. Maniv, I. Diamant, I. Neder, S. Wiedmann, V.K. Guduru, F. Chiappini, U. Zeitler, J.C. Maan, K. Chashka, A. Kanigel, Y. Dagan, Probing the surface states in Bi_2Se_3 using the Shubnikov–de Haas effect, Phys. Rev. B 86 (2012) 045131, http://dx.doi.org/10.1103/PhysRevB.86.045131.

[24] M. Chrobak, K. Mackosz, M. Jurczyszyn, M. Dobrzanski, K. Nowak, T. Slezak, M. Zajac, M. Sikora, M. Rams, T. Eelbo, J. Stepien, M. Wasniowska, O. Mathon, F. Yakhou-Harris, D.G. Merkel, I. Miotkowski, Z. Kakol, A. Kozlowski, M. Przybylski, Z. Tarnawski, Fe dopants and surface adatoms versus nontrivial topology of single-crystalline Bi_2Se_3, New J. Phys. 22 (6) (2020) 063020, http://dx.doi.org/10.1088/1367-2630/ab890d.

[25] K. Nowak, M. Jurczyszyn, M. Chrobak, K. Maćkosz, A. Naumov, N. Olszowska, M. Rosmus, I. Miotkowski, A. Kozłowski, M. Sikora, M. Przybylski, Influence of doping on the topological surface states of crystalline Bi_2Se_3 topological insulators, Materials 15 (6) (2022) 2083, http://dx.doi.org/10.3390/ma15062083.

[26] V.A. Kulbachinskii, A.Y. Kaminskii, V.G. Kytin, A.d. Visser, Thermoelectric power and Shubnikov-de Haas effect in magnetic impurity-doped Bi_2Te_3 and Bi_2Se_3, J. Magn. Magn. Mater. 272–276 (2004) 1991–1992, http://dx.doi.org/10.1016/j.jmmm.2003.12.787.

[27] D. Shoenberg, Magnetic Oscillations in Metals, in: Cambridge Monographs on Physics, Cambridge University Press, 1984, http://dx.doi.org/10.1017/CBO9780511897870.

[28] J.P. Heremans, W. Bartłomiej, Tetradymites: Bi_2Te_3-related materials, in: Materials Aspect of Thermoelectricity, CRC Press, Taylor & Francis, CRC Press is an imprint of the Taylor & Francis Group, and informa business, 2017.

[29] B.J. Lawson, Y.S. Hor, L. Li, Quantum oscillations in the topological superconductor candidate $Cu_{0.25}Bi_2Se_3$, Phys. Rev. Lett. 109 (2012) 226406, http://dx.doi.org/10.1103/PhysRevLett.109.226406.